Petroleum Science 20 (2023) 2809–2821

Contents lists available at ScienceDirect

Petroleum Science

journal homepage: www.keaipublishing.com/en/journals/petroleum-science

Original Paper

Model-constrained and data-driven double-supervision acoustic impedance inversion

Dong-Feng Zhao [a], Na-Xia Yang [a], Jin-Liang Xiong [b], Guo-Fa Li [a, *], Shu-Wen Guo [c]

[a] State Key Laboratory of Petroleum Resources and Prospecting, China University of Petroleum, Beijing, 102249, China
[b] Dagang Oil Field, PetroChina, Tianjin, 300280, China
[c] Research Institute of Exploration and Development, Dagang Oil Field, PetroChina, Tianjin, 300280, China

ARTICLE INFO

Article history:
Received 24 July 2022
Received in revised form
3 January 2023
Accepted 22 March 2023
Available online 4 April 2023

Edited by Jie Hao

Keywords:
Acoustic impedance inversion
Model constraints
Double supervision
BiLSTM neural network
Reservoir structure characterization

ABSTRACT

Seismic impedance inversion is an important technique for structure identification and reservoir prediction. Model-based and data-driven impedance inversion are the commonly used inversion methods. In practice, the geophysical inversion problem is essentially an ill-posedness problem, which means that there are many solutions corresponding to the same seismic data. Therefore, regularization schemes, which can provide stable and unique inversion results to some extent, have been introduced into the objective function as constrain terms. Among them, given a low-frequency initial impedance model is the most commonly used regularization method, which can provide a smooth and stable solution. However, this model-based inversion method relies heavily on the initial model and the inversion result is band limited to the effective frequency bandwidth of seismic data, which cannot effectively improve the seismic vertical resolution and is difficult to be applied to complex structural regions. Therefore, we propose a data-driven approach for high-resolution impedance inversion based on the bidirectional long short-term memory recurrent neural network, which regards seismic data as time-series rather than image-like patches. Compared with the model-based inversion method, the data-driven approach provides higher resolution inversion results, which demonstrates the effectiveness of the data-driven method for recovering the high-frequency components. However, judging from the inversion results for characterization the spatial distribution of thin-layer sands, the accuracy of high-frequency components is difficult to guarantee. Therefore, we add the model constraint to the objective function to overcome the shortages of relying only on the data-driven schemes. First, constructing the supervisor1 based on the bidirectional long short-term memory recurrent neural network, which provides the predicted impedance with higher resolution. Then, convolution constraint as supervisor2 is introduced into the objective function to guarantee the reliability and accuracy of the inversion results, which makes the synthetic seismic data obtained from the inversion result consistent with the input data. Finally, we test the proposed scheme based on the synthetic and field seismic data. Compared to model-based and purely data-driven impedance inversion methods, the proposed approach provides more accurate and reliable inversion results while with higher vertical resolution and better spatial continuity. The inversion results accurately characterize the spatial distribution relationship of thin sands. The model tests demonstrate that the model-constrained and data-driven impedance inversion scheme can effectively improve the thin-layer structure characterization based on the seismic data. Moreover, tests on the oil field data indicate the practicality and adaptability of the proposed method.

© 2023 The Authors. Publishing services by Elsevier B.V. on behalf of KeAi Communications Co. Ltd. This is an open access article under the CC BY-NC-ND license (http://creativecommons.org/licenses/by-nc-nd/4.0/).

1. Introduction

Seismic inversion plays an important role in subsurface spatial geometric characterization (e.g., the reservoir thickness, lateral distributions, superimposed relationships) and reservoir physical properties evaluation (e.g., porosity, fluid saturation) (Lelièvre and

* Corresponding author.
E-mail address: lgfseismic@126.com (G.-F. Li).

https://doi.org/10.1016/j.petsci.2023.03.019
1995-8226/© 2023 The Authors. Publishing services by Elsevier B.V. on behalf of KeAi Communications Co. Ltd. This is an open access article under the CC BY-NC-ND license (http://creativecommons.org/licenses/by-nc-nd/4.0/).

Oldenburg, 2009; Mavko et al., 2009). As an essential technical approach, acoustic impedance inversion is mostly used method for hydrocarbon and mineral exploration. Over the past few decades, numerous impedance inversion methods have been proposed for reservoir characterization (Singleton, 2008; Tetyukhina et al., 2010; Xiang et al., 2021). However, due to the limited frequency bandwidth of the acquired seismic data, it is far from satisfying the resolution requirements of thin-layer sandstone characterization. Consequently, applying a suitable inversion scheme to accurately recover the high-frequency components is particularly important for acoustic impedance inversion and quantitative seismic interpretation (Wang et al., 2021a; Zhu and Gibson, 2016). According to the different degrees of dependence on data, impedance inversion can be divided into three categories, including model-based impedance inversion, data-driven intelligent inversion, and data-driven and model-constrained double-supervision inversion scheme. Theoretically, data-driven intelligent inversion approach can provide impedance inversion results with higher resolution compared to the model-based inversion method. However, without clear physical meaning, networks have not interpretability, the inversion results are difficult to evaluate, weak generalization ability and adaptability weaken the further application and development of data-driven inversion methods. The model-based acoustic impedance inversion is still the most popular and useful method for practical field application.

Geophysical inversion problems are often seriously ill-posed due to the noise contamination and limited seismic frequency bandwidth, there are many impedance models that can approximately explain the same seismic records (Tarantola, 2005). Moreover, it is not enough to detailed characterize the geological structures based on the seismic data with limited bandwidth. Therefore, the development of the acoustic impedance inversion aims to obtain unique and stable inversion results with higher resolution. In order to overcome the ill-posedness of impedance inversion, regularization terms are introduced into the objective function by imposing the inversion results to follow the expected distribution features to obtain a specific solution (Liu and Yin, 2015; Gholami and Siahkoohi, 2010; Wang et al., 2020; He et al., 2022). The introduction of the prior information (e.g., borehole data, geological and statistical characteristics) can narrow the solution space and provide a compromise solution between the expected model and observed seismic records. The smooth constraint is the most commonly used regularization scheme (Tikhonov, 1963; Tikhonov and Arsenin, 1977), which can effectively stabilize the solution by minimizing the l_2 norm of the gradient for the estimated parameter. The inversion results can be used to describe the variation tendency of the estimated parameter while is difficult to characterize the small-scale structures. Therefore, the regularization method is proposed and applied to improve the resolution of the inversion results by assuming that the inverted model has sparse gradients (Alemie and Sacchi, 2011; Gholami, 2015). This blocky regularizations use the l_1 norm to produce blocky solutions, which can properly preserve the edges and discontinuities. Further, in recent years, more complex regularization schemes (e.g., $l_{1,2}$ mixed norm) have been proposed to consider the blocky and continuous features of subsurface geological structures simultaneously (Chen et al., 2016; Pérez et al., 2017). The challenges of these inversion approaches are that they only suitable for specific blocks with single geological characteristics. In addition, choosing an appropriate algorithm to solve the objective function is also important.

Even with the introduction of regularization terms, the model-based inversion results are still difficult to satisfy the resolution requirements for thin-layer structure characterization. With the successful application of deep learning technologies in the field of geophysics (e.g., first-break picking, seismic noise attenuation, seismic facies classification, fault identification, velocity modeling, wavefield simulation, high-resolution processing, seismic data interpolation, local slope estimation, reservoir characterization) (Zwartjes and Yoo, 2022; Gao et al., 2021, 2022; Silva et al., 2020; Fabien-Outllet and Sarkar, 2020; Siahkoohi et al., 2019; Chai et al., 2021; Yoon et al., 2021; Huang et al., 2021; Zhang and Alkhalifah, 2020; Zhu et al., 2020; Chen et al., 2020), the data-driven impedance inversion is applied for obtaining high-resolution reservoir structures (Wang et al., 2021b; Meng et al., 2022; She et al., 2019). Das et al. (2019) perform the impedance inversion experiments based on the convolutional neural networks (CNNs) and evaluate the robustness of the method. Mustafa et al. (2019) use 1-D temporal convolutional network (TCN) to predict acoustic impedance by posing the inversion problem as sequence modeling, which successfully captures the long-term trends. Furthermore, without known wavelet, Guo et al. (2019) obtain the predicted impedance with good lateral continuity based on the bidirectional long short-term memory (BiLSTM) network. Different from the CNNs, the BiLSTM neural network introduces the internal correlation between adjacent hidden layers which treat seismic data as sequences of time-series data rather than image-like patches. Moreover, the introduction of gating system and cell state alleviates the gradient problem caused by long-term dependence. In recent years, the evaluation and analysis of high-resolution inversion results from the data-driven methods have become important. The introduction of model constraints and prior information improve the credibility of the inversion results and the interpretability of the neural network models to some extent. Yuan et al. (2019) construct a prior constraint using the long-wavelength information from full-waveform inversion(FWI) for poststack impedance inversion, which yields a broadband predicted impedance. Song et al. (2021) train the network model by the way of semi-supervised learning to overcome the limited labeled data. Wang et al. (2022) adopt the Robinson convolutional model to simulate the seismic forward process and constrain the inversion process. In addition, bilateral filtering is applied to guarantee the spatial continuity of the inversion results. Incorporating model constraints into the deep-learning impedance inversion schemes further improves the reliability and accuracy of inversion results.

In this paper, we propose a novel approach for post-stack acoustic impedance inversion based on the BiLSTM neural network model. We first train the BiLSTM neural network by using seismic traces and corresponding impedance labels. Then, we test the effectiveness of the proposed method for high-frequency component recovery. Compared with the model-based impedance inversion, the BiLSTM neural network model can evidently enhance the resolution of the inversion results benefitting from multiple nonlinear calculations. However, due to the weak generalization ability and adaptability of deep learning technologies, it is difficult to guarantee the accuracy of the high-frequency components of the inversion results. Therefore, we introduce the convolution constrains into the objective function to overcome this shortage. The predicted impedance based on the BiLSTM neural network is converted into the reflectivity series and then convolved with the wavelet matrix of the forward model. The synthetic seismic records and the input seismic traces form an error term to correct the inversion results. Finally, we test the proposed method on model data and filed data, the results show that introducing model constraints into the data-driven inversion scheme not only improves the resolution of the inversion results, but also ensures the accuracy and reliability of the inversion results.

Data-driven inversion methods are difficult to interpret due to unclear physical meaning. The introduction of model constraint guarantees the reliability of solution and makes the BiLSTM neural

network easier to understand. In double-supervision inversion scheme, the BiLSTM neural network model plays the role of an approximate inverse operator similar to the traditional model-based impedance inversion approach, which convert the input seismic traces into the impedance data. In addition, the proposed method has more adaptability and fewer assumptions than model-based inversion.

This paper is organized as follows. First, we compare the traditional model-based impedance inversion method with the data-driven supervised impedance inversion approach. Second, we introduce the basic principles of the BiLSTM neural network and conduct experiments based on the model data. Then, the convolution model is introduced into the objective function to guarantee the accuracy of the inversion results. The data-driven and model-constrained double-supervision acoustic impedance inversion scheme is developed. We compare the inversion effects of these three methods based on the model data. Finally, the field data tests are conducted to illustrate and demonstrate the potential and effectiveness of the proposed method for complex geologic zones.

2. Theory

2.1. Model-based impedance inversion

Model-based impedance inversion is one of the most commonly used post-stack linearized impedance inversion method. The prior knowledge or expectations of geological model are introduced into the objective function to obtain a stable and specific solution. Based on the convolutional theory (Yilmaz, 2001), the single-trace seismic record can be expressed as the convolution of seismic wavelet with reflectivity series.

$$\mathbf{d} = \mathbf{W}\mathbf{r} + \mathbf{n} \tag{1}$$

where $\mathbf{d}$ is the observed seismic data, $\mathbf{W}$ is the known wavelet matrix, $\mathbf{r}$ represents the underground reflectivity series and $\mathbf{n}$ denotes the random noise. For post-stack seismic data, it is approximated that the reflection coefficient is determined by the impedance of the strata above and below the interface.

$$r_i = \frac{Z_{i+1} - Z_i}{Z_{i+1} + Z_i} \tag{2}$$

In general, the amplitude of reflectivity is no longer than 0.3 (Walker and Ulrych, 1983). Therefore, the reflectivity can be linearized expressed approximately by acoustic impedance as following equation.

$$r_i \approx \frac{\Delta \ln(Z_i)}{2} = \frac{1}{2}(\ln(Z_{i+1}) - \ln(Z_i)) \tag{3}$$

where Z is the acoustic impedance, i represents the interface between the strata i and $i+1$. Then, Eq. (1) can be expressed in matrix form as follows (Stolt and Weglein, 1985; Russell and Hampson, 1991)

$$\underbrace{\begin{bmatrix} d_1 \\ d_2 \\ \vdots \\ d_n \end{bmatrix}}_{\mathbf{d}} = \underbrace{\frac{1}{2}\begin{bmatrix} w_1 & 0 & \cdots & 0 \\ \vdots & w_1 & \ddots & \vdots \\ w_k & \vdots & \ddots & 0 \\ 0 & w_k & \vdots & w_1 \\ \vdots & \ddots & \ddots & \vdots \\ 0 & \cdots & 0 & w_k \end{bmatrix}\begin{bmatrix} -1 & 1 & 0 & \cdots & 0 \\ 0 & -1 & 1 & \ddots & 0 \\ \vdots & \ddots & \ddots & \ddots & \vdots \\ 0 & \cdots & 0 & -1 & 1 \end{bmatrix}}_{\mathbf{G}}\underbrace{\begin{bmatrix} m_1 \\ m_2 \\ \vdots \\ m_n \end{bmatrix}}_{\mathbf{m}} \tag{4}$$

where $\mathbf{m}$ is the natural logarithmic impedance. For simplicity, we define the linearized forward operator as

$$\mathbf{G} = \frac{1}{2}\mathbf{W}\mathbf{D} \tag{5}$$

where $\mathbf{D}$ denotes the first-order difference matrix. The relationship between seismic data $\mathbf{d}$ and natural logarithmic impedance $\mathbf{m}$ can be rewritten as (Buland and More, 2003)

$$\mathbf{d} = \mathbf{G}\mathbf{m} + \mathbf{n} \tag{6}$$

The post-stack impedance inversion aims to estimate $\mathbf{m}$ from known seismic records $\mathbf{d}$. However, due to the ill-posedness of the inverse problem, there are multiple solutions to Eq. (6) Model-based impedance inversion method obtains stable and unique solutions by giving a low-frequency initial model, which derived from the low-pass filtering of interpolation and extrapolation of well logging data. The objective function for impedance inversion can be written as

$$J(\mathbf{m}) = \min_{\mathbf{m}} \ ||\mathbf{d} - \mathbf{G}\mathbf{m}||_2^2 + \lambda||\mathbf{m} - \mathbf{m}_0||_2^2 \tag{7}$$

where $||\bullet||_p$ denotes the p norm, $\mathbf{m}_0$ is the low-frequency initial model, λ is a trade-off parameter used for controlling the contribution of the initial model for inversion result, which is determined by multiple trials. The solution to Eq. (7) can be obtained based on the iterative algorithm and is presented as

$$\mathbf{m} = (\mathbf{G}^T\mathbf{G} + \lambda\mathbf{I})^{-1}(\mathbf{G}^T\mathbf{d} + \lambda\mathbf{m}_0) \tag{8}$$

Given a low-frequency initial model, model-based impedance inversion can obtain an unique and smooth solution. In addition, another most commonly used regularization scheme is to enforce the impedance $\mathbf{m}$ to have a sparse gradient. The regularization terms include some prior knowledge or expectations about the unknown parameter, therefore, a more general expression for model-based impedance inversion is written as follows

$$\widehat{\mathbf{m}} = \arg\min_{\mathbf{m}} \ \{||\mathbf{d} - \mathbf{G}\mathbf{m}||_2^2 + \lambda f(m)\} \tag{9}$$

where $f(m)$ is the regularization term and presents additional cognition. By introducing a regularization term, model-based impedance inversion can obtain a stable unique solution. Nevertheless, the solution depends heavily on the quality of the seismic data, the initial model, the extracted wavelets and inversion algorithms(Yuan et al., 2022). The enhancement of resolution and characterization of thin-layer structures based on the inversion result is still limited.

2.2. Data-driven impedance inversion

The inversion results of the model-based impedance inversion method are band limited to the effective frequency bandwidth of raw seismic data. This restriction means that model-based impedance inversion cannot evidently improve the resolution of inversion results and effectively describe the spatial distribution of thin-layer sand bodies. Therefore, we propose a data-driven inversion approach based on the BiLSTM neural network. Different from the model-based inversion scheme, data-driven methods have strong power to learn and represent high-level features, which is another effective scheme to improve the characterization of subsurface structures (Kim and Nakata, 2018; Wu et al., 2020, 2022).

The LSTM model is a variant network of the basic RNN, which contains four special connection patterns in one LSTM unit. The introduction of gates enables the LSTM to handle the long-term

dependencies and alleviate the overfitting problems (Williams and Zipser, 1989; Hochreiter, 1998; Hochreiter and Schmidhuber, 1997). The calculation of current time step includes the filtered information of the previous time step and input new information. The introduction of cell state gives the LSTM memory function and provides a path for information transmission. Meanwhile, which information will be reserved is decided through a gating system. The forget gate is used to retain the memory information and the input gate handles the current input sequence information, while the output gate is used to calculate the unit output. These three gates are associated by the cell state for entire information processing in one LSTM unit. Updating the cell state is the key for LSTM to deal with long sequence data. Fig. 1 shows the internal structures of an LSTM cell unit. The specific calculation process is as follows

$$\mathbf{f}_t = \sigma(\mathbf{W}_f \mathbf{x}_t + \mathbf{U}_f \mathbf{h}_{t-1} + \mathbf{b}_f) \tag{10}$$

$$\mathbf{i}_t = \sigma(\mathbf{W}_i \mathbf{x}_t + \mathbf{U}_i \mathbf{h}_{t-1} + \mathbf{b}_i) \tag{11}$$

$$\mathbf{o}_t = \sigma(\mathbf{W}_o \mathbf{x}_t + \mathbf{U}_o \mathbf{h}_{t-1} + \mathbf{b}_o) \tag{12}$$

$$\mathbf{g}_t = \tanh(\mathbf{W}_g \mathbf{x}_t + \mathbf{U}_g \mathbf{h}_{t-1} + \mathbf{b}_g) \tag{13}$$

$$\mathbf{c}_t = \mathbf{f}_t \odot \mathbf{c}_{t-1} + \mathbf{i}_t \odot \mathbf{g}_t \tag{14}$$

$$\mathbf{h}_t = \mathbf{o}_t \odot \tanh(\mathbf{c}_t) \tag{15}$$

$$\mathbf{y}_t = \mathbf{W}_y \mathbf{h}_t + \mathbf{b}_y \tag{16}$$

where the cell state $\mathbf{c}_t$ and hidden state $\mathbf{h}_t$ are updated by input gate $\mathbf{i}_t$, forget gate $\mathbf{f}_t$ and output gate $\mathbf{o}_t$. σ is a sigmoid activation function, its output value is between 0 and 1, 0 presents discard and 1 means reserve, which is used for three gates to select information. $\mathbf{W}$, $\mathbf{U}$ and $\mathbf{b}$ are the weight coefficient matrix and the bias vector, $\odot$ is the Hadamard product, denotes elementwise multiply for two matrix. tanh is another activation function, which is used for cell state update and information output.

Stacking two LSTM units as one hidden layer for processing both forward and reverse sequence data constitutes a BiLSTM neural network (Schuster and Paliwal, 1997). In this way, the output of the current time step not only considers the information of the previous time step, but also selects the information from the future.

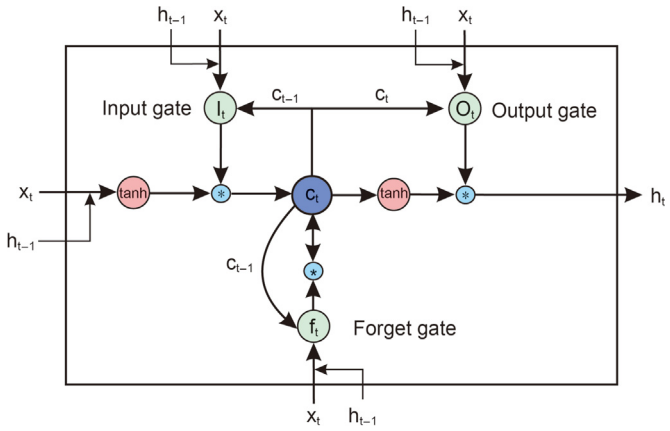

Fig. 1. Internal structure of an LSTM unit. The current input sequence data $\mathbf{x}_t$ and previous hidden state $\mathbf{h}_{t-1}$ are processed by the input gate, forget gate, cell state and output gate for updating the hidden layer state, which control the input, discard, transfer and output of information.

Fig. 2 shows the data processing process of the BiLSTM neural network. In current time step, the hidden state $\mathbf{h}_t$ is a concatenated matrix from two opposite directions as follows

$$\mathbf{h}_t = [\overrightarrow{\mathbf{h}_t}, \overleftarrow{\mathbf{h}_t}] \tag{17}$$

where $\overrightarrow{\mathbf{h}_t}$ denotes the forward hidden state and $\overleftarrow{\mathbf{h}_t}$ presents the backward hidden state. The computation of the output vector $\mathbf{y}_t$ and other parameters are consistent with LSTM.

To determine the optimal neural network architectures and hyperparameters, we chose the MSE as the objective function F and minimize it.

$$F = \frac{1}{N}\sum_{i=1}^{N}(\mathbf{Z}_i - \widehat{\mathbf{Z}}_i)^2 \tag{18}$$

where N represents the number of samples, the $\mathbf{Z}_i$ and $\widehat{\mathbf{Z}}_i$ denote the true and predicted impedance, respectively. Fig. 3 displays the schematic of high-resolution impedance inversion based on the BiLSTM neural network. At time step i, the input seismic waveforms $x = \{x_1, x_2, \ldots, x_t\}$, which is mapped to a specific impedance label through a designed network configurations. The high-resolution inversion results are obtained by compressing the seismic waveforms to a great extent.

2.3. Model-constrained and data-driven impedance inversion

Benefiting from the powerful nonlinear mapping capability of the deep learning technique, the data-driven method can significantly improve the resolution of impedance inversion results and recover the high-frequency components outside the effective frequency bandwidth of seismic data. However, same as the model-based impedance inversion technical scheme, it is still difficult to guarantee whether the high-frequency components of the inversion results is accurate and reliable. Different from the model-based impedance inversion, deep learning techniques have no clear physical meaning and weak generalization ability, it is difficult to accurately and comprehensively evaluate the inversion results. Therefore, it is important to improve the reliability of impedance prediction results of the BiLSTM neural network. Consequently, in addition to constructing the BiLSTM neural network as supervisor1 to provide the predicted impedance with higher resolution. We introduce the convolution model as supervisor2 in the objective function to ensure that the synthetic seismic data from the predicted impedance is consistent with the input seismic data, thereby improving the reliability of the inversion results. Fig. 4 shows the framework of the model-constrained and data-driven impedance inversion technology. The objective function of the double-supervised inversion scheme is mathematically defined as

$$L(\widehat{\mathbf{Z}}) = \min_{\mathbf{Z}} \underbrace{\left\|\mathbf{Z} - \widehat{\mathbf{Z}}\right\|_2^2}_{\text{data}} + \lambda \underbrace{\left\|\mathbf{d} - \mathbf{W}\widehat{\mathbf{r}}\right\|_2^2}_{\text{model}}$$

$$\widehat{r}_i = \frac{\widehat{Z}_{i+1} - \widehat{Z}_i}{\widehat{Z}_{i+1} + \widehat{Z}_i} \tag{19}$$

where $\{\mathbf{d},\mathbf{Z}\}$ is the input data of the BiLSTM neural network, $\widehat{\mathbf{Z}}$ represents the predicted impedance, $\mathbf{W}$ denotes the wavelet matrix used for convolutional forward model, $\widehat{\mathbf{r}}$ is the reflectivity series calculated based on the predicted impedance and λ represents the regularization parameter used to balance the weights between the

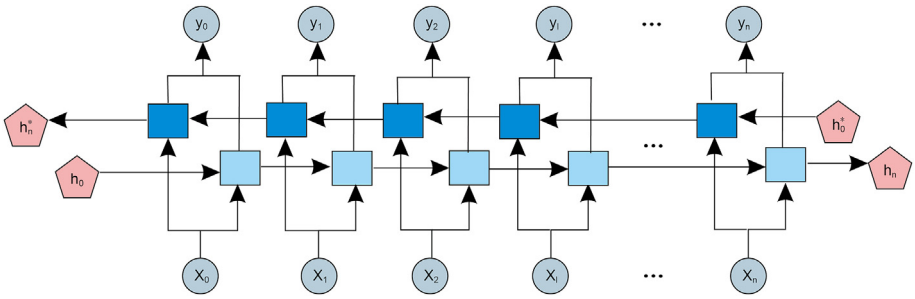

Fig. 2. Schematic of the BiLSTM neural network model. The forward vector **x** and inverse vector **x** are input into the network simultaneously, output the predicted vector **y** after the hidden state **h** and cell state are adjusted and updated.

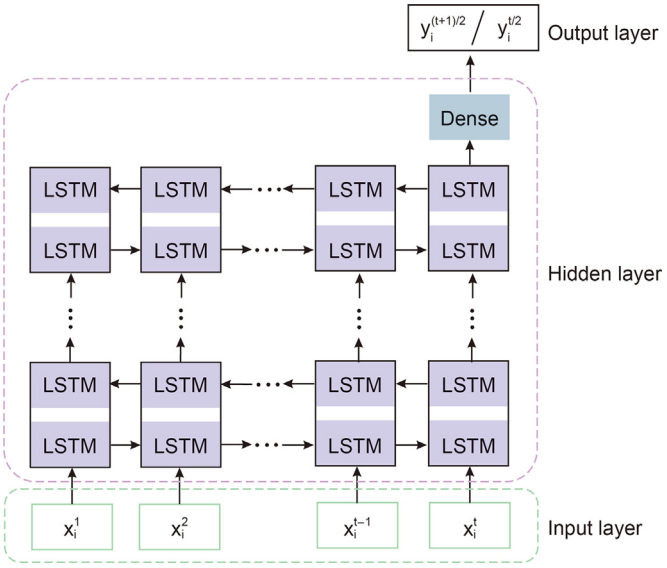

Fig. 3. The configuration of the BiLSTM neural network model, which consist of the input layer, hidden layer and output layer. Each hidden layer is composed of two LSTM unit for processing the forward and inverse input seismic data simultaneously. Where *t* represents the time step, the vector $\mathbf{x_i}$ and $\mathbf{y_i}$ represent the input seismic data and the predicted acoustic impedance, respectively.

predicted impedance error (the first term of Eq. (19) or supervisor1) and the synthetic data error (the second term of Eq. (19) or supervisor2).

In this case, the BiLSTM neural network plays the role of approximate inverse operator, which converts the input seismic data into impedance with higher resolution than the model-based inversion method. When λ equals to zero, only the impedance labels constrain the inversion process. The inversion results depend heavily on the generalization ability and adaptability of the neural network. When λ is larger than zero, the convolutional forward model is introduced into the objective function to guarantee the consistency between the synthetic seismic data of the inverted impedance and the input raw seismic data. Due to the same forward model and wavelet matrix are used, the introduction of supervisor2 further improves the reliability of the inversion results. Compared with the model-based impedance inversion method, this data-driven and model-constrained double-supervision inversion scheme provides higher resolution inversion results, which takes fully advantages of the ability of deep learning techniques to characterize nonlinear relationships. The high-frequency components can be effectively recovered. Different from the pure data-driven approach, the introduction of model constraints enables the inversion result more reliable and accurate, which further reduces the multiplicity of the inversion results and the dependency of the neural network. The concise workflow of the data-driven and model-constrained double-supervision impedance inversion scheme is summarized in Table 1.

3. Model analysis

3.1. Model-based impedance inversion

In order to test the proposed method, we construct a thin sand

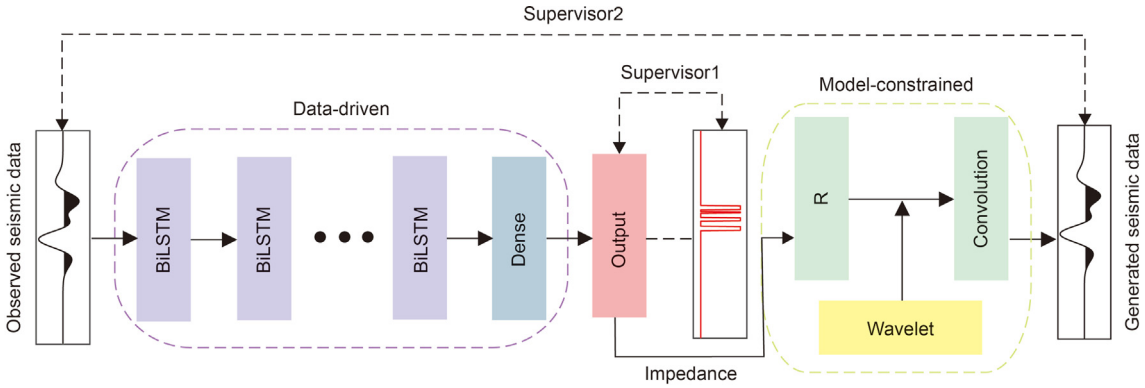

Fig. 4. The framework of the model-constrained and data-driven double-supervision acoustic impedance inversion approach. Six BiLSTM and one dense layer form the supervisor1. The final dense layer in the data-driven scheme can linearly weight the extracted features to convert them into acoustic impedance and compare with the label data. The synthetic seismic data from the predicted impedance and input seismic data form the supervisor2 where the wavelet matrix is the same as the forward model. Supervisor1 and supervisor2 are used to provide high-resolution impedance results and minimize the predictive error, respectively.

Table 1
The workflow of the data-driven and model-constrained double-supervision acoustic impedance inversion.

impedance inversion.
Input: wavelet matrix **W**, training data set $\{\mathbf{d},\mathbf{m}\}_T$, validation data set $\{\mathbf{d},\mathbf{m}\}_V$, the regularization parameter λ, the batch size b, the numbers of LSTMs c, the number of neurons for each layers e, the time step t, learning rate l and the training epochs n.
Output: High-resolution inverted impedance $\widehat{\mathbf{m}}$.
Stage 1: Prepare training data and normalize data
1: Prepare the training data set $\{\mathbf{d},\mathbf{m}\}_T$ and validation data set $\{\mathbf{d},\mathbf{m}\}_V$ from the model or field data;
2: Standardize all data and labels by using the Min-Max normalization;
Stage 2: Train the BiLSTM neural network
3: set hyperparameters b, c, e, t, l, n;
4: **for** $i = 1$: n
5: Evaluate the data-driven inversion results according to equation (18) and judge whether the hyperparameters are appropriate;
6: **end for**
7: Repeat steps 3–6 until the optimal BiLSTM configurations is obtained;
Stage 3: Introduce the model constrain
8: set the weight parameter λ;
9: **for** $i = 1$: n
10: According to the equation19 to evaluate the effect of model constraint;
11: **end for**
12: Repeat steps 8–11 until the suitable λ is obtained;
Stage 4: Implement impedance inversion using the double-supervision scheme
13: Implement the impedance inversion based on the model or field data;
14: Inverse normalization of the prediction results.

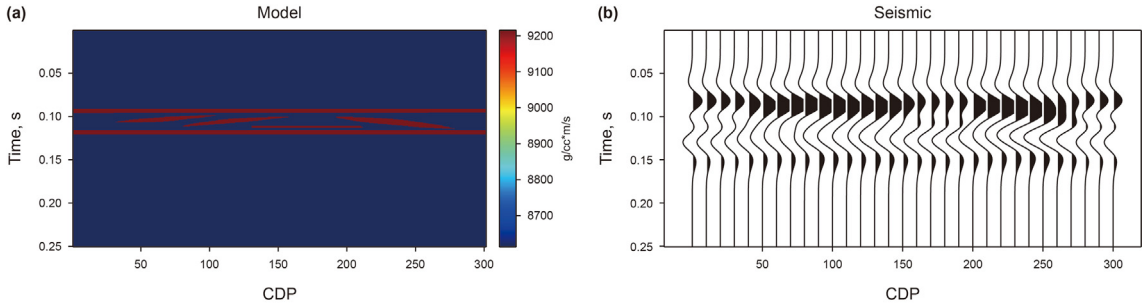

Fig. 5. The model data used to test the validity and performance of the BiLSTM neural network on high-resolution acoustic impedance inversion. (a) Impedance data as training label and (b) corresponding seismic data convolved with 15Hz Ricker wavelet as training data.

model (see Fig. 5), which consists of 301 × 501 (seismic traces × time samples) data points with sampling interval of 0.5 ms. The velocity of the sand is 3800 m/s and is 3600 m/s for the shale. The time thickness of the horizontal sand is about 5ms and is about 2.5 ms for the middle thin-layer sand. The synthetic seismic records is convolved with the 15Hz Ricker wavelet. Due to the severe interference effects, it is difficult to identify the spatial structure of the thin-layer sand and characterize the spatial distribution of sand body based on the seismic records. Therefore, we carry out the log-constrained acoustic impedance inversion experiment, and further characterize and illustrate the thin-layer structure based on the inversion results.

The log-constrained acoustic impedance inversion method, which firstly is to establish the initial model by interpolating along the geological horizons according to the well logging data (Li et al., 2008; Morozov and Ma, 2009; Kroode et al., 2013). The convolution algorithm is then used to generate the synthetic seismic records from the initial model and seismic wavelet. Finally, the error between the synthetic seismic records and the observed seismic data is calculated, and the impedance model is continuously corrected and updated through error back propagation algorithm. When the error of these two meets the accuracy requirements, we obtain and output the final result of the acoustic impedance inversion. We select five impedance traces (cdp 20, 60, 120, 180, 240) from the geological model as pseudo-logging data for the log-constrained impedance inversion. First, the geological horizon interpretation is performed based on seismic data and prior knowledge. Then, we construct the low-frequency initial model based on the low-pass filtering of the well log interpolation results. Finally, we construct the objective function of the log-constrained acoustic impedance inversion method as shown in Eq. (7), the corresponding inversion result is obtained according to the inversion algorithm shown in Eq. (18). In order to make full use of the high-frequency information provided by the well logging data, we also implement an impedance inversion test based on the full-frequency band initial model, which directly use the interpolation results of the logging data as initial model. Fig. 6 shows the inversion initial models and corresponding inversion results, respectively.

The results of these set of the acoustic impedance inversion experiments based on different initial models show that the inversion results based on the log-constrained impedance inversion approach are difficult to accurately describe and characterize the spatial structure characteristics of thin-layer sand bodies. Regardless of which initial model is used, the inversion results cannot effectively describe the spatial distributions and superposition relationships of sand bodies. The resolution of the inversion results is limited by the seismic frequency bandwidth and the initial model. The log-constrained impedance inversion approach, which is categorized as linear inversion. The nature of linear inversion method is that it can only provide frequency components

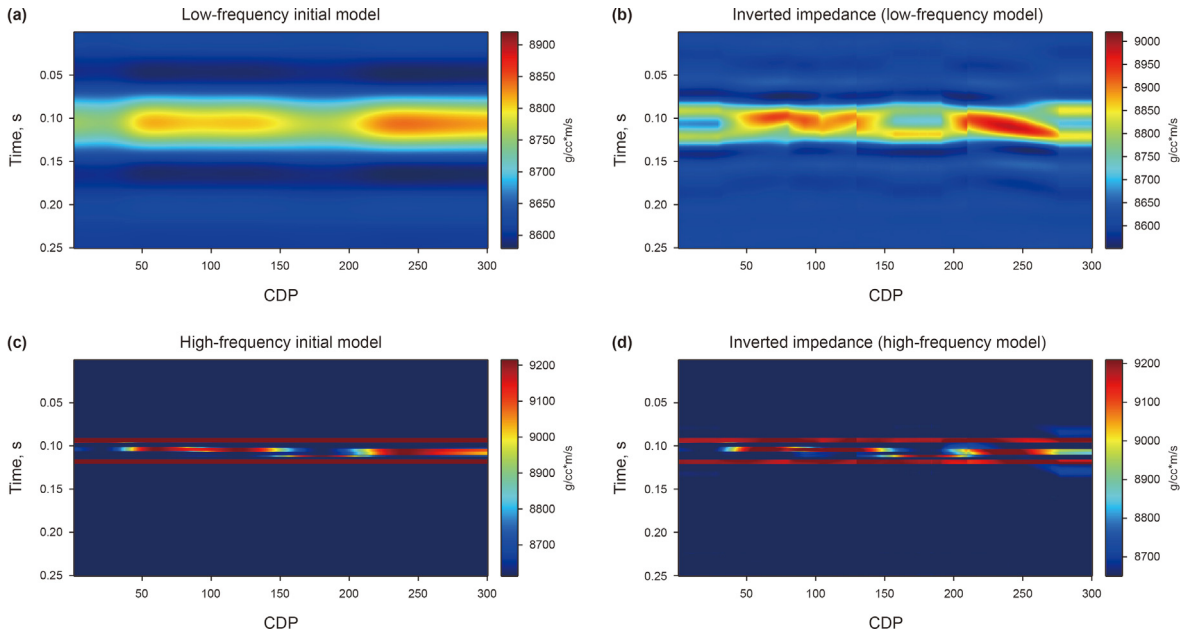

Fig. 6. The log-constrained acoustic impedance inversion results. (a) The low-frequency initial model and (b) corresponding inversion result. (c) The full-frequency initial model and (d) corresponding inversion result.

within the seismic frequency bandwidth (Li et al., 2011; Cooke and Schneider, 1983; Assis et al., 2019). Due to the difficulty in enhancing the resolution of the inversion results, the log-constrained inversion based on the low-frequency initial model is greatly limited in the characterization of thin-layer structures. Although the inversion result based on the full-frequency band initial model has higher resolution intuitively, the inversion result outside wells is more derived from the interpolation and extrapolation of the initial model, which fails to accurately characterize the lateral distribution and spatial variation for sand bodies.

3.2. BiLSTM-based impedance inversion

The above test results show that the model-based impedance inversion method itself cannot recover the high-frequency components, and the high-frequency information is completely derived from the initial model. Therefore, we carry out the data-driven impedance inversion experiment based on the BiLSTM neural network. We select five seismic traces (cdp 20, 60, 120, 180, 240) and corresponding impedance data as input for network training, which is consistent with the data used to build the initial model in the model-based impedance inversion. After min-max normalization, the data are divided into the training data sets and validation data sets according to the ratio of 75%: 25%. The training set is used to train the model and determine the hyperparameters, whereas the validation set is used to judge whether it is overfitting and to evaluate the accuracy of the model.

For determining the optimal neural network architectures, we conduct a series of hyperparameter experiments, the Adam optimization algorithm is used to update the gradients and adjust the weights and biases of each neurons. The stage1 and stage2 displayed in Table 1 illustrate the specific experimental procedure. For the most important parameters: learning rate l (control the speed of gradient update) and time step t (the length of the input data), we set a series values to evaluate the performance of l{0.01, 0.005, 0.0025, 0.001, 0.00025} and t{16, 24, 32, 48, 64} for the network model. Fig. 7 shows the error of the network on the validation set with different hyperparameters. The other parameters are determined in the same way. Table 2 gives the parameter values for the trained BiLSTM neural network model.

After obtaining the optimal network configurations, we perform the impedance inversion on the entire model data based on the BiLSTM model. The MSE error is 0.1573 and 0.2635 for the training set and validation set, respectively, which demonstrates the feasibility and acceptability of the BiLSTM-based impedance inversion scheme. Fig. 8 shows the predicted impedance. Compared with the results from the low-frequency model-based impedance inversion, the data-driven BiLSTM-based inversion approach significantly improves the resolution of the inversion results. The inversion results accurately distinguish the superposition relationship of thin sands, the distribution characteristics of the top and bottom horizontal sands are clear. However, for the lens sandstone between the top and bottom layered sand, the inversion results cannot accurately describe the lateral distribution ranges and characterize the lens boundaries as high-frequency model-based inversion result. It is difficult to evaluate which of these two methods is better and which is worse. This exposes the inherent flaws of purely data-driven inversion methods, the weak generalization ability and adaptability limit the further application and development of the network model for oil field data. Therefore, we introduce the convolution constraint into the objective function to improve the reliability of the data-driven BiLSTM-based inversion results.

3.3. Double-supervision impedance inversion

The convolution constraint is used to control the entire inversion process as supervisor2. Specifically, the predicted impedance provided by the BiLSTM network model is converted into the reflectivity series and convolved with the wavelet matrix, and the resulting synthetic seismic records are compared with the input seismic data. This process optimizes the supervisor1 and improves the predictive accuracy of the network. The network architectures and hyperparameters are the same as the above data-driven impedance inversion method, where we only add the constraint term to the loss function and determine the trade-off parameter λ based on the stages3 displayed in Table 1 we set a series of values of

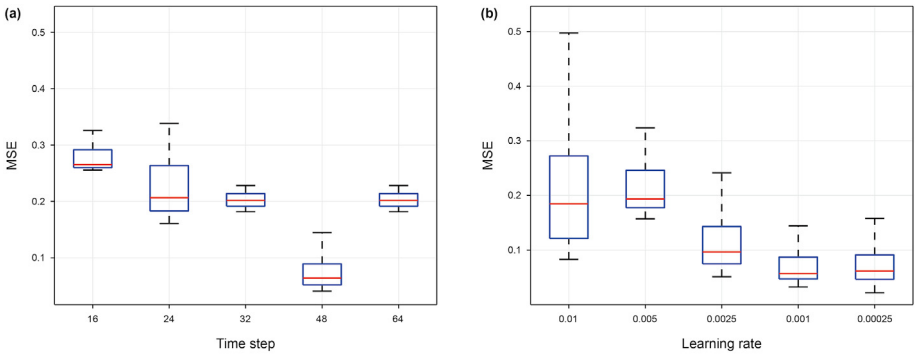

Fig. 7. Train and adjust the hyperparameters of the BiLSTM neural network based on the model data, the MSE on the validation data sets is used to evaluate and determine the (a) time step and (b) learning rate.

Table 2
Hyperparameter values for the trained BiLSTM neural network model.

Parameter	Description	Value
b	batch_size	128
c	the number of hidden layers (LSTM)	6
e	the number of neurons for each hidden layer	128 + 32+8 + 8+32 + 128
t	time step	48
l	learning rate	0.001
n	training epochs	500

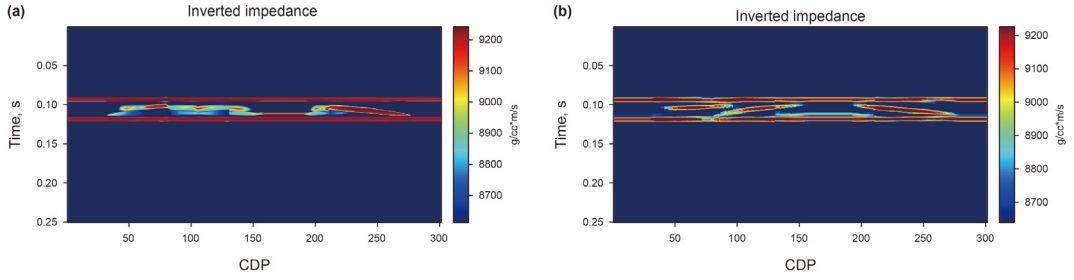

Fig. 8. Acoustic impedance inversion results based on the model data from the (a) data-driven inversion method and (b) model-constrained and data-driven inversion scheme.

λ(0.5, 0.1, 0.05, 0.01, 0.001) to balance the weights of the convolution constraints. According to the network performance on the validation data set, we determine the optimal values of λ is 0.01 and conduct the impedance inversion on the entire model data.

The inversion result of double-supervision impedance inversion, which not only retains the high-resolution effect of the data-driven method, but also ensures the accuracy of the inversion result under the supervision of convolution constraints (Fig. 8). Specifically, in addition to the clear distribution characteristics of the top and bottom sandstones, the lateral distribution of the thin sandstone and lens sandstone in the middle are accurately described, the superposition relationship of the sandstone is clearly distinguished, sand boundaries are distinctly delineated. Compared with the data-driven inversion method based on the BiLSTM neural network, the data-driven inversion with model constraints can more accurately describe the thin-layer spatial structures. The predictive error of the model-constrained and data-driven impedance inversion scheme is 0.0712 and 0.1063 on the training data set and validation data set displayed in Table 3, respectively. The relative error amplification on the validation set is 67.5% and 49.3% of the data-driven and double-supervision impedance inversion schemes. In addition to the training error being significantly smaller than that of the pure data-driven inversion method, the double-supervision inversion approach also further reduces the error difference between the training set and the validation set, which demonstrates that the introduction of convolution constraint alleviates the overfitting problem to some extent. Fig. 9 also illustrates this well, which shows the learning curves of the training data sets and validation data sets for the double-supervision impedance inversion scheme. Although the validation loss is slightly larger than the training error, it decreases steadily and does not increase over the limited training epochs, which indicates that the BiLSTM neural network model is not overfitted and the hyperparameter settings is appropriate. This will further improve and enhance the generalization ability and adaptability of the proposed BiLSTM neural network in field application.

Table 3
Comparison of prediction errors for different inversion methods.

Schemes	MSE	
	training	validation
data-driven	0.1573	0.2635
model-constrained and data-driven	0.0712	0.1063

In this section, we compare the performance of three different acoustic impedance inversion methods on model data. The experimental results show that the model-driven impedance inversion

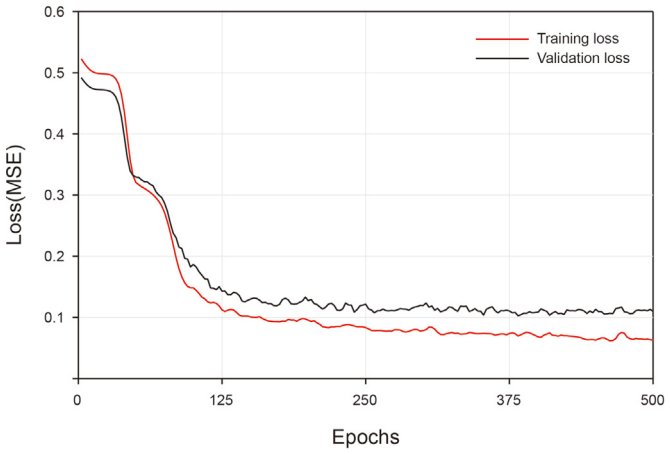

Fig. 9. Learning curves of the training data sets (red) and validation data sets (black) for the model-constrained and data-driven double-supervision acoustic impedance inversion method.

itself cannot recover the missing high-frequency components in the acquired seismic data, and the inversion results are heavily dependent on the initial model. The data-driven inversion method benefits from the powerful nonlinear mapping capabilities of deep learning techniques, which can greatly improve the resolution of the inversion results and restore the high-frequency components. Meanwhile, the proposed BiLSTM-based data-driven acoustic impedance inversion approach has certain noise resistance and robustness(Fig. 10). However, such methods generally lack the measurement and evaluation of the reliability of high-frequency components. The double-supervised impedance inversion based on data-driven and model-constrained approach combines the advantages of both, that is, it significantly improves the characterization and description effect for thin-layer structures while ensures the accuracy of high-frequency components.

4. Field example

In order to further evaluate the transfer and generalization ability and its applicability and practicality of the proposed method in oil field data, we conduct a more comprehensive test and analysis with X oil field data. Fig. 11 displays the tectonic setting of the study area. The main target layer in this area is the Y Formation, which is buried to a shallow depth of about 1100–1500 m. The main oil and gas resources are concentrated in the second member of the Y Formation. The Y Formation in this area is in a wet period in the early stage, which is the alluvial fans and braided river depositions near the provenance. The channel is wide, the sand bodies are widely distributed with large sedimentary thickness. In the middle and late stages, meandering river deposits are formed after entering the dry season. The width of the channel gradually narrows as it moves away from the provenance and the sedimentary thickness of the sand body decreases. The second member of Y Formation is dominated by meandering river deposits. The main controlling factor of lithologic oil and gas reservoirs depends on the lithology of the reservoir, which is highly heterogeneous. It needs the suitable depth to form lithologic traps in different depositional environments. If the deposition depth is too large, the necessary reservoir formation conditions will be lacking, and if the deposition depth is too small, the necessary cap rock sealing conditions will be lacking. The mudstone deposited in the second member of the Y Formation creates good sealing conditions for the oil and gas reservoir regions. Therefore, lithologic oil and gas reservoirs dominated by lithologic pinchouts and sandstone lenses can be formed.

We adopt the network structure of the model test with fine-tuned the node weights for acoustic impedance inversion of oil field seismic data. The area enclosed by the red dotted line is the target zone with 6 well distributed (Fig. 11), where A-D and F are used for re-training the proposed neural network model to get the new weight matrix and bias parameters. The remaining well (E) is used as a blind well to evaluate and validate the reliability and practicality of the proposed method. The impedance logs derived

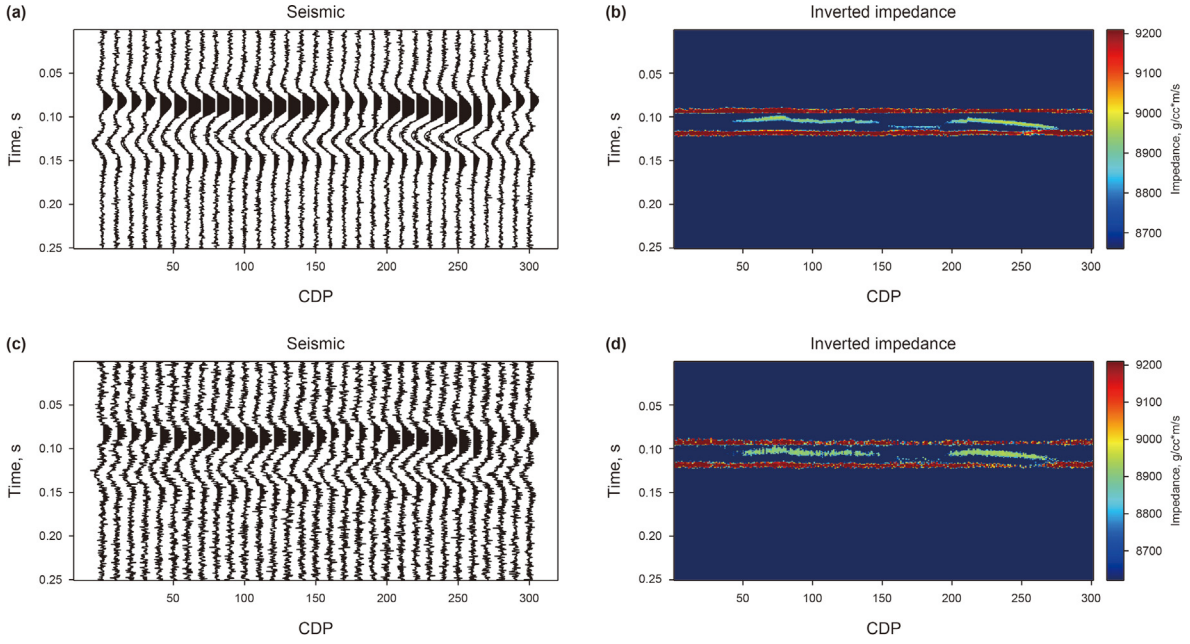

Fig. 10. The noise resistance tests of the proposed data-driven inversion method based on the model data. (a) Synthetic seismic records with a signal-to-noise ratio (SNR) of 10 and its corresponding impedance inversion profile (b). (c)The seismic data (SNR = 5) and (d) corresponding inversion result.

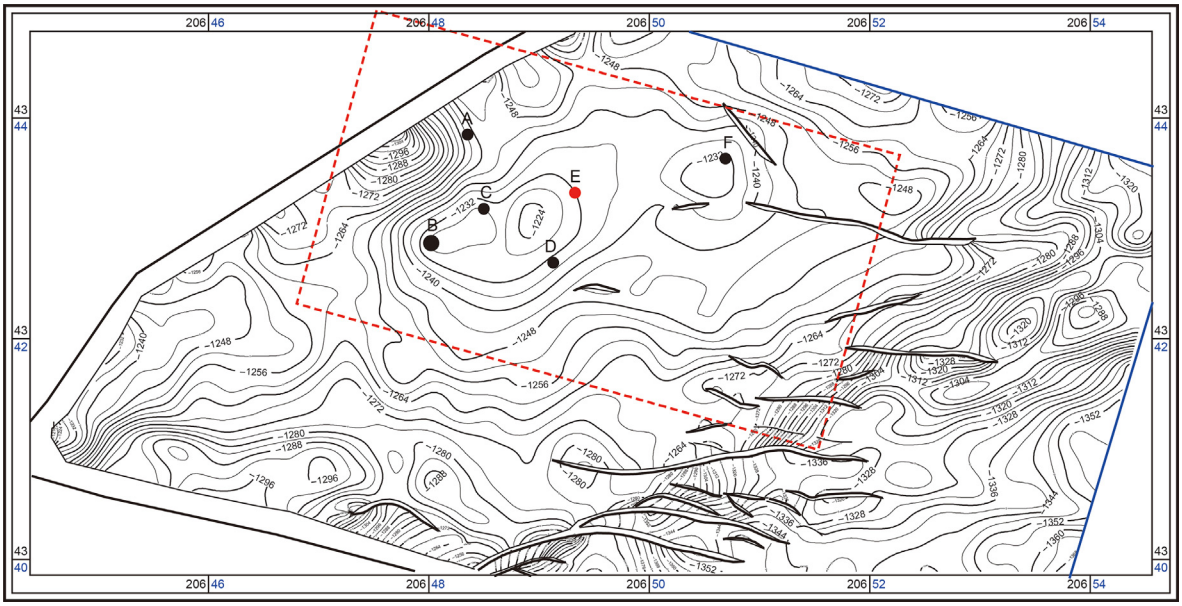

Fig. 11. The tectonic setting under the study area with the target zone enclosed with red dotted line and six well locations, where A-D and F are used for re-training, E is used as a blind well to verify the practicability and applicability of the proposed inversion scheme.

from the sonic- and density-log measurements are resampled to 2ms and fed into the BiLSTM neural network model along with the well-side seismic records as training data to obtain the appropriate weights for each neurons. Fig. 12 is the seismic section from the target zone used to verify the validity and generalization ability of the double-supervision impedance inversion scheme. The data consist of 91 seismic traces and 51 time samples with an interval of 2ms. Fig. 13 displays the acoustic impedance inversion results of the log-constrained impedance inversion, the data-driven impedance inversion and the proposed model-constrained and data-driven double-supervision impedance inversion scheme. The inserted impedance log is from the blind well E and is used for intuitively evaluating the inversion result. Consistent with the conclusions obtained from the model experiment, the proposed double-supervision acoustic impedance inversion scheme provides inversion results with higher resolution and better characterization for thin-layer sand bodies. The lateral distributions and superposition relationships of sand bodies are clearer and more accurate. The correlations between the inversion results and the impedance log of the blind well are 62.4%, 78.8% and 86.2%, respectively. In order to illustrate and demonstrate the effectiveness of the proposed scheme in describing the spatial structure of sand bodies, we

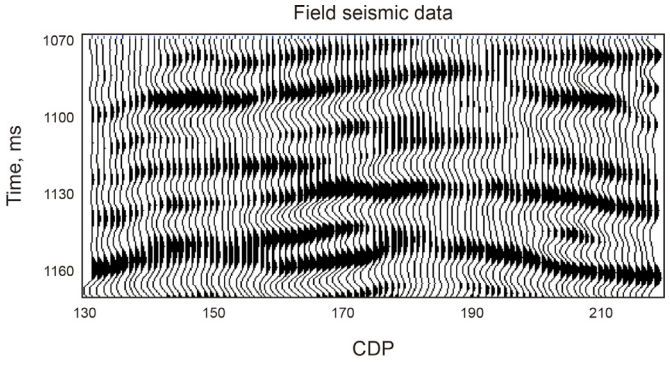

Fig. 12. The oil field seismic section used for verifying the proposed double-driven acoustic impedance inversion scheme.

extract the impedance slices of the target layer as shown in Fig. 14. The outline of the river delineated by the white dotted line fully illustrates the effectiveness of the proposed method in characterizing the spatial distribution for the channel sand. The inversion results of the double-supervision scheme not only greatly improve the resolution requirements of thin-layer structure characterization, but also overcome the weak spatial continuity of log-constrained acoustic impedance inversion approach, which has important practical significance and application potential for thin-layer structure characterization based on seismic data.

Compared with the log-constrained acoustic impedance inversion method, the data-driven inversion scheme provides higher resolution inversion results. The inversion result breaks the limitation of the seismic effective frequency bandwidth, and effectively recovers the missing high-frequency information, which has important implications for the characterization of thin-layer spatial structures. By introducing a convolution-constrained regularization term into the BiLSTM-based inversion function, the seismic records synthesized by the predicted impedance and the observed seismic traces constitute the error term to constrain the inversion process, which is used to ensure the reliability and accuracy of the inversion results. The experimental results show that the introduction of the convolution model alleviates the weak horizontal continuity of the sand body in the model-based inversion method to certain extent, which accurately describes the lateral distribution of the sand body while improving the resolution. The impedance inversion tests based on field seismic data further illustrates that the double-supervision acoustic impedance inversion scheme is more effective and accurate for the characterization and description of channel sand bodies.

5. Conclusions

In this paper, we propose an acoustic impedance inversion method based on the BiLSTM neural network model. Compared with the conventional model-based impedance inversion, the data-driven inversion approach can provide high-resolution inversion results without solving complex objective function. Seismic traces are treated as time-series data rather than image-like patches to

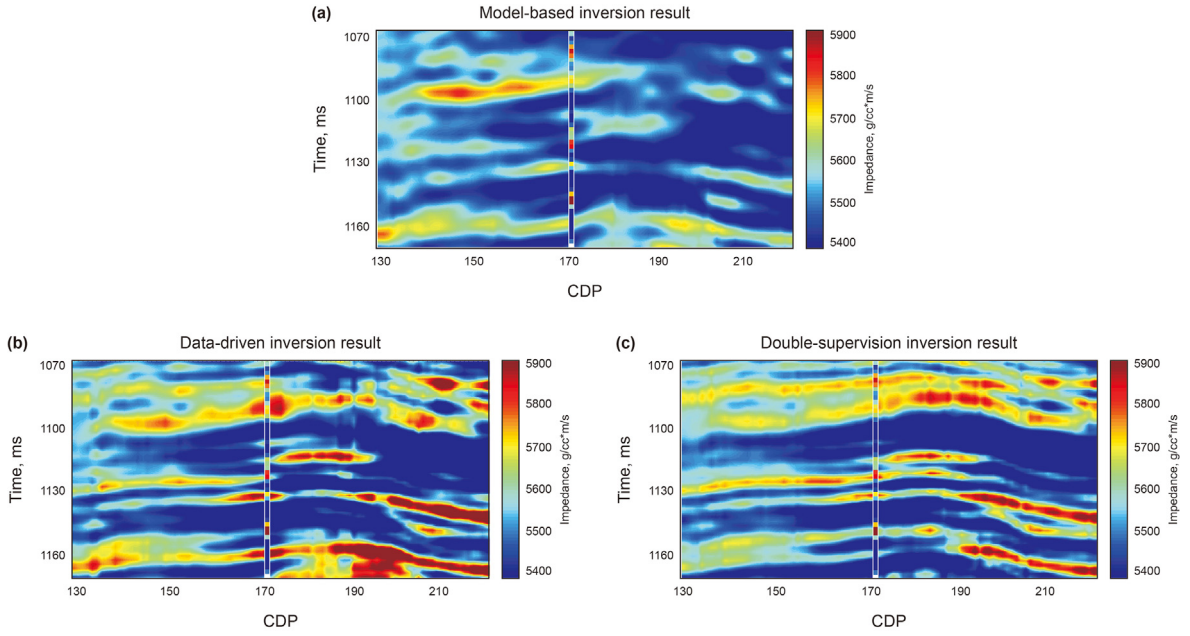

Fig. 13. Comparisons between acoustic impedance inversion results from (a) the model-driven inversion approach, (b) data-driven impedance inversion method and (c) the proposed double-supervision acoustic impedance inversion scheme based on the field seismic data. The inserted impedance log is derived from the sonic- and density-log measurements, which is used as a blind well to verify the accuracy and reliability of the inversion results.

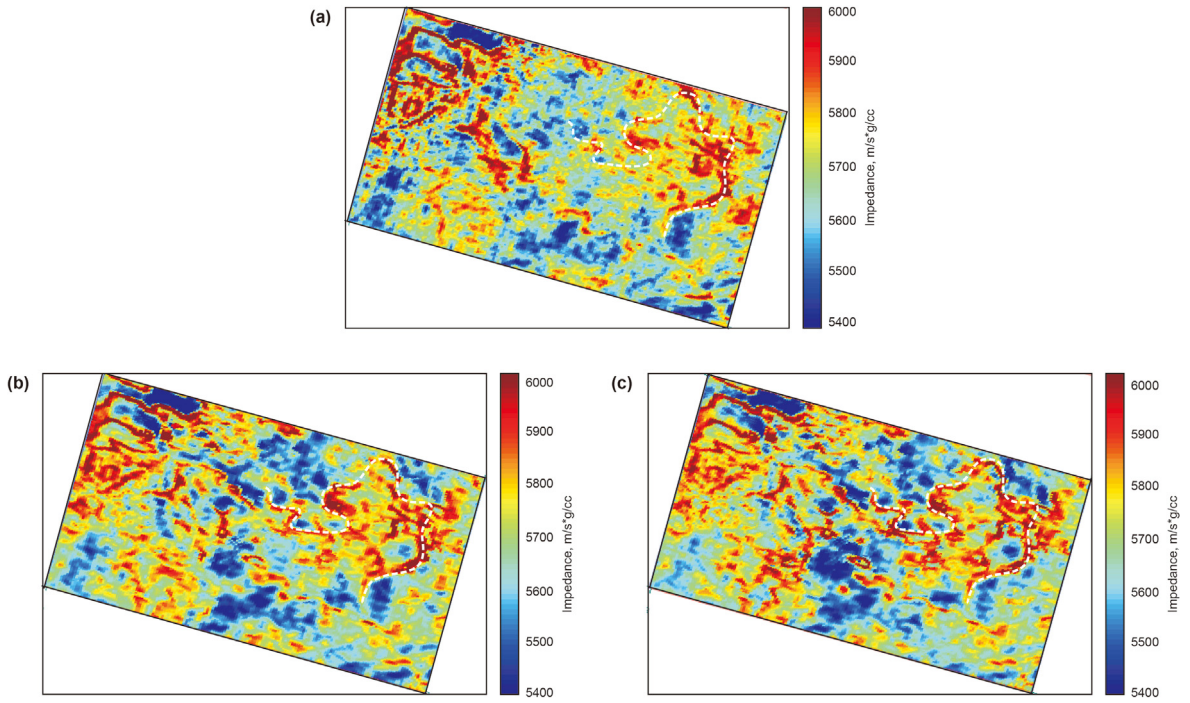

Fig. 14. Impedance slices for (a) model-driven inversion result, (b) data-driven impedance inversion result and (c) double-driven inversion result. The outline of the river delineated by the white dotted line further illustrates the effectiveness of the model-constrained and data-driven double-supervision impedance inversion scheme for spatial structure characterization of sand bodies.

input the BiLSTM model for training, which preserves the small-scale structures and reflects the continuous variations of impedance data simultaneously. In addition, we introduce the model constrains into the loss function to guarantee the accuracy and reliability of the recovered high-frequency components. When the wavelet matrix is known, the synthetic seismic data calculated from the predicted impedance and the input seismic data constitute the error term that is used to constrain the training process of the BiLSTM neural network. In this case, the BiLSTM model is similar to the inverse operator that converts seismic records into impedance data, which makes the network easier to understand. The proposed method is tested with model data and field data and compared with the model-based impedance inversion. The results show that the model-based impedance inversion

method cannot efficiently recover the high-frequency components outside the seismic frequency bandwidth, and the inversion results depend heavily on the initial model. Compared with model-based impedance inversion, the data-driven inversion algorithm based on the BiLSTM neural network only relies on the information of seismic data itself without external intervention, which can provide inversion results with higher resolution and can deal with the complex geological zones. Furthermore, the incorporation of the convolution model in the objective function significantly reduces the inversion error. The model test results demonstrate the effectiveness of the proposed method for improving the inversion accuracy and reliability. Moreover, inversion results of the field data further indicate the effectiveness and adaptability of the proposed model-constrained and data-driven double-supervision impedance inversion scheme.

Declaration of competing interest

We declare that we have no financial and personal relationships with other people or organizations that can inappropriately influence our work, there is no professional or other personal interest of any nature or kind in any product, service and/or company that could be construed as influencing the position presented in, or the review of, the manuscript entitled “Model-constrained and data-driven double-supervision acoustic impedance inversion”.

Acknowledgments

The study was funded by R&D Department of China National Petroleum Corporation (2022DQ0604-04), the Strategic Cooperation Technology Projects of CNPC and CUPB (ZLZX2020-03), and the Science Research and Technology Development of PetroChina (2021DJ1206).

References

Alemie, W., Sacchi, M.D., 2011. High-resolution three-term AVO inversion by means of a Trivariate Cauchy probability distribution. Geophysics 76, R43–R55. https://doi.org/10.1190/1.3554627.

Assis, C.A.M., Santos, H.B., Schleicher, J., 2019. Colored and linear inversions to relative acoustic impedance. Geophysics 84, N15–N27. https://doi.org/10.1190/geo2018-0185.1.

Buland, A., More, H., 2003. Bayesian linearized AVO inversion. Geophysics 68, 185–198. https://doi.org/10.1190/1.1543206.

Chai, X.T., Tang, G.Y., Lin, K., Yan, Z., Gu, H.M., Peng, R.H., Sun, X.D., Cao, W.J., 2021. Deep learning for multitrace sparse-spike deconvolution. Geophysics 86, V207–V218. https://doi.org/10.1190/geo2020-0342.1.

Chen, W., Yang, L.Q., Zha, B., Zhang, M., Chen, Y.K., 2020. Deep learning reservoir porosity prediction based on multilayer long short-term memory network. Geophysics 85, WA213–WA225. https://doi.org/10.1190/geo2019-0261.1.

Chen, Y., Chen, H., Xiang, K., Chen, X., 2016. Geological structure guided well log interpolation for high-fidelity full waveform inversion. Geophys. J. Int. 207, 1313–1331. https://doi.org/10.1093/gji/ggw343.

Cooke, D.A., Schneider, W.A., 1983. Generalized linear inversion of reflection seismic data. Geophysics 48, 655–795. https://doi.org/10.1190/1.1441497.

Das, V., Pollack, A., Wollner, U., Mukerji, T., 2019. Convolutional neural network for seismic impedance inversion. Geophysics 84, R869–R880. https://doi.org/10.1190/geo2018-0838.1.

Fabien-Outllet, G., Sarkar, R., 2020. Seismic velocity estimation: a deep recurrent neural-network approach. Geophysics 85, U21–U29. https://doi.org/10.1190/geo2018-0786.1.

Gao, K., Huang, L.J., Zheng, Y.C., Lin, R.R., Hu, H., Cladohous, T., 2022. Automatic fault detection on seismic images using a multiscale attenutaion convulutional neural network. Geophysics 87, N13–N29. https://doi.org/10.1190/geo2020-0945.1.

Gao, Y., Zhao, P.Q., Li, G.F., Li, H., 2021. Seismic noise attenuation by signal reconstruction: an unspervised machine learning approach. Geophys. Prospect. 69, 984–1002. https://doi.org/10.1111/1365-2478.13070.

Gholami, A., 2015. Nonlinear multichannel impedance inversion by total-variation regularizaiton. Geophysics 80, R217–R224. https://doi.org/10.1190/geo2015-0004.1.

Gholami, A., Siahkoohi, H., 2010. Regularization of linear and non-linear geophysical ill-posed problems with joint sparsity constraints. Geophys. J. Int. 180, 871–882. https://doi.org/10.1111/j.1365-246X.2009.04453.x.

Guo, R., Zhang, J.J., Liu, D., Zhang, Y.B., Zhang, D.W., 2019. Application of Bi-directional long short-term memory recurrent neural network for seismic impedance inversion: 81st Annual International Conference and Exhibition. EAGE, Expanded Abstracts 1–5. https://doi.org/10.3997/2214-4609.201901386.

He, L.S., Wu, H., Wen, X.T., You, J.C., 2022. Seismic acoustic impedance inversion using reweighted L1-norm sparse constraint. Geosci. Rem. Sens. Lett. IEEE 19, 1–5. https://doi.org/10.1109/LGRS.2022.3168015.

Hochreiter, S., 1998. The vanishing gradient problem during learning recurrent neural nets and problem solutions. Int. J. Uncertain. Fuzziness Knowledge-Based Syst. 6, 107–116. https://doi.org/10.1142/S0218488598000094.

Hochreiter, S., Schmidhuber, J., 1997. Long short-term memory. Neural Comput. 9, 1735–1780. https://doi.org/10.1162/neco.1997.9.8.1735.

Huang, W.L., Gao, F., Liao, J.P., Chuai, X.Y., 2021. A deep learning network for estimation of seismic local slopes. Petrol. Sci. 18, 92–105. https://doi.org/10.1007/s12182-020-00530-1.

Kim, Y., Nakata, N., 2018. Geophysical inversion versus machine learning in inverse problems. Lead. Edge 37, 894–901. https://doi.org/10.1190/tle37120894.1.

Kroode, F.T., Bergler, S., Corsten, C., Maag, J.W.D., Strijbos, F., Tijhof, H., 2013. Broadband seismic data-the importance of low frequencies. Geophysics 78. https://doi.org/10.1190/geo2012-0294.1. WA3–WA14.

Lelièvre, P.G., Oldenburg, D.W., 2009. A comprehensive study of including structural orientation information in geophysical inversions. Geophys. J. Int. 178, 623–637. https://doi.org/10.1111/j.1365-246X.2009.04188.x.

Li, G.F., Li, H., Ma, Y.Y., Xiong, J.L., 2011. Analysis of the ambiguity of log-constrained seismic impedance inversion. Petrol. Sci. 8, 151–156. https://doi.org/10.1007/s12182-011-0128-y.

Li, G.F., Xiong, J.L., Zhou, H., Zhai, T.L., 2008. Seismic reflection characteristics of fluvial sand and shale interbedded layers. Appl. Geophys. 5, 219–229. https://doi.org/10.1007/s11770-008-0025-3.

Liu, X., Yin, X., 2015. Blocky Inversion with Total Variation Regularization and Bounds Constraint: 85th Annual International Meeting. SEG, Expanded Abstracts, pp. 3497–3501. https://doi.org/10.1190/segam2015-5832614.1.

Mavko, G., Mukerji, T., Dvorkin, J., 2009. The Rock Physics Handbook, second ed. Cambrideg University Press. https://doi.org/10.1017/CBO9780511626753.

Meng, D.L., Wu, B.Y., Wang, Z.G., Zhu, Z.L., 2022. Seismic impedance inversion using conditional generative adversarial network. Geosci. Rem. Sens. Lett. IEEE 19, 1–5. https://doi.org/10.1109/LGRS.2021.3090108.

Morozov, I.B., Ma, J.F., 2009. Accurate poststack acoustic-impedance inversion by well-log cailbration. Geophysics 74, R59–R67. https://doi.org/10.1190/1.3170687.

Mustafa, A., Alfarraj, M., Airegib, G., 2019. Estimation of Acoustic Impedance from Seismic Data Using Temporal Convolutional Network: 89th Annual International Meeting. SEG, Expanded Abstracts, pp. 2554–2558. https://doi.org/10.1190/segam2019-3216840.1.

Pérez, D.O., Velid, D.R., Sacchi, M.D., 2017. Three-term inversion of prestack seismic data using a weighted l2, 1 mixed norm. Geophys. Prospect. 65, 1477–1495. https://doi.org/10.1111/1365-2478.12500.

Russell, B., Hampson, D., 1991. Comparison of Poststack Seismic Inversion Methods: 61st Annual International Meeting. SEG, Expanded Abstracts, pp. 876–878. https://doi.org/10.1190/1.1888870.

Schuster, M., Paliwal, K.K., 1997. Bidirectional recurrent neural networks. IEEE Trans. Signal Process. 45, 2673–2681. https://doi.org/10.1109/78.650093.

She, B., Wang, Y.J., Liu, Z.N., Cai, H.P., Liu, W., Hu, G.M., 2019. Seismic impedance inversion using dictionary learning-based sparse representation and nonlocal similarity. Interpretation 7. https://doi.org/10.1190/int-2018-0196.1. SE51–SE67.

Siahkoohi, A., Louboutin, M., Heremann, F.J., 2019. The importance of transfer learning in seismic modeling and imaging. Geophysics 84, A47–A52. https://doi.org/10.1190/geo2019-0056.1.

Silva, A.A., Tavares, M.W., Carrasquilla, A., Misságia, R., Ceia, M., 2020. Petrofacies classification using machine learning algorithms. Geophysics 85, WA101–WA113. https://doi.org/10.1190/geo2019-0439.1.

Singleton, S., 2008. The use of seismic attenuation to aid simultaneous impedance inversion in geophysical reservoir characterization. Lead. Edge 27, 398–407. https://doi.org/10.1190/1.2896633.

Song, L., Yin, X.Y., Zong, Z.Y., Li, B.K., Qu, X.Y., Xi, X.P., 2021. Deep learning seismic impedance inversion based on prior constraints. Oil Geophys. Prospect. 56, 716–727. https://doi.org/10.13810/j.cnki.issn.1000-7210.2021.04.005.

Stolt, R.H., Weglein, A.B., 1985. Migration and inversion of seismic data. Geophysics 50, 2458–2472. https://doi.org/10.1190/1.1441877.

Tarantola, A., 2005. Inverse Problem Theory and Methods for Model Parameter Estimation. SIAM. https://doi.org/10.1137/1.9780898717921.

Tetyukhina, D., van Vliet, L.J., Luthi, S.M., Wapenaar, K., 2010. High-resolution reservoir characterization by an acoustic impedance inversion of a Tertiary deltaic clinoform system in the North Sea. Geophysics 75, O57–O67. https://doi.org/10.1190/1.3506039.

Tikhonov, A., 1963. Solution of incorrectly formulated problems and the regularization method. Sovit Math. Doklady. 4, 1035–1038.

Tikhonov, A., Arsenin, V.Y., 1977. Methods for Solving Ill-Posed Problems. John Wiley and Sons Inc. https://doi.org/10.1137/1021044.

Walker, C., Ulrych, T.J., 1983. Autoregressive recovery of the acoustic impedance. Geophysics 48, 1338–1350. https://doi.org/10.1190/1.1441414.

Wang, L.Q., Zhou, H., Liu, W.L., Yu, B., He, H.L., Chen, H.M., Wang, N., 2021a. Data-driven multichannel poststack sesimic impedance inversion via patch-ordering regularization. Geophysics 86, R197–R210. https://doi.org/10.1190/geo2020-0253.1.

Wang, L.Q., Zhou, H., Liu, W.L., Yu, B., Zhang, S., 2021b. High-resolution seismic acoustic impedance inversion with the sparsity-based statistical model. Geophysics 86, R509–R527. https://doi.org/10.1190/geo2020-0345.1.
Wang, Y.Q., Wang, Q., Lu, W.K., Li, H.S., 2022. Physics-constrained seismic impedance inversion based on deep learning. Geosci. Rem. Sens. Lett. IEEE 19, 1–5. https://doi.org/10.1109/LGRS.2021.3072132.
Wang, Z., Gao, J., Chen, H., Pan, X., Lin, J., 2020. Multichannel blind acoustic impedance inversion based on 2D-TV regularization: annual International Conference and Exhibition Online, EAGE. Expand. Abstr. 1–5. https://doi.org/10.3997/2214-4609.202010623.
Williams, R.J., Zipser, D., 1989. A learning algorithm for continually running fully recurrent neural network. Neural Comput. 1, 270–280. https://doi.org/10.1162/neco.1989.1.2.270.
Wu, B.Y., Meng, D.L., Wang, L.L., Liu, N.H., Wang, Y., 2020. Seismic impedance inversion using fully convolutional residual network and transfer learning. Geosci. Rem. Sens. Lett. IEEE 17, 2140–2144. https://doi.org/10.1109/LGRS.2019.2963106.
Wu, B.Y., Xie, Q., Wu, B.H., 2022. Seismic impedance inversion based on residual attention network. IEEE Trans. Geosci. Rem. Sens. 60, 1–17. https://doi.org/10.1109/TGRS.2022.3193563.
Xiang, K., Yang, Y.D., Huang, H.D., Luo, Y.N., Jiang, M.Q., 2021. Joint impedance inversion and spectral decomposition for deepwater gas reservoir characterization: a case study in South China Sea. Interpretation 9, T63–T77. https://doi.org/10.1190/int-2019-0135.1.
Yilmaz, O., 2001. Seismic Data Analysis: Processing, Inversion, and Interpretation of Seismic Data. Society of Exploration Geophysicists. https://doi.org/10.1190/1.9781560801580.
Yoon, D., Yeeh, Z., Byun, J., 2021. Seismic data reconstruction using deep bidirectional long short-term memory with skip connections. Geosci. Rem. Sens. Lett. IEEE 18, 1298–1302. https://doi.org/10.1109/LGRS.2020.2993847.
Yuan, S.Y., Jiao, X.Q., Luo, Y.N., Sang, W.J., Wang, S.X., 2022. Double-scale supervised inversion with a data-driven forward model for low-frequency impedance recovery. Geophysics 87, R165–R181. https://doi.org/10.1190/geo2020-0421.1.
Yuan, S.Y., Wang, S.Y., Luo, Y.N., Wei, W.W., Wang, G.C., 2019. Impedance inversion by using the low-frequency full-waveform inversion result as an a prior model. Geophysics 84, R149–R164. https://doi.org/10.1190/geo2017-0643.1.
Zhang, Z.D., Alkhalifah, T., 2020. High-resolution reservoir characterization using deep learning-aided elastic full-waveform inversion: the North Sea field data example. Geophysics 85, WA137–WA146. https://doi.org/10.1190/geo2019-0340.1.
Zhu, D., Gibson, R., 2016. Seismic Inversion and Uncertainty Analysis Using a Transdimensional Markov Chain Monte Carlo Method: 86th Annual International Meeting. SEG, Expanded Abstracts, pp. 3666–3671. https://doi.org/10.1190/segam2016-13870581.1.
Zhu, W., Li, X., Liu, C., Xue, F.Z., Han, Y.F., 2020. An STFT-LSTM system for P-wave identification. Geosci. Rem. Sens. Lett. IEEE 17, 19–23. https://doi.org/10.1109/LGRS.2019.2922536.
Zwartjes, P., Yoo, J., 2022. First break picking with deep learning-evaluation of network architectures. Geophys. Prospect. 70, 318–342. https://doi.org/10.1111/1365-2478.13162.